Physalis mottle virus-like nanocarriers with expanded internal loading capacity

Krister J. Barkovich[1]*, Zhuohong Wu[2,3], Zhongchao Zhao[2,3], Andrea Simms[2,3], Eric Y. Chang[1,4], Nicole F. Steinmetz[1,2,3,5,6,7,8]*

[1] Department of Radiology, University of California, San Diego, San Diego, CA
[2] Department of NanoEngineering, University of California, San Diego, San Diego, CA
[3] Center for Nano-ImmunoEngineering, University of California, San Diego, San Diego, CA
[4] Radiology Service, VA San Diego Healthcare System, San Diego, CA
[5] Department of Bioengineering, University of California, San Diego, San Diego, CA
[6] Institute for Materials Discovery and Design, University of California, San Diego, CA
[7] Moores Cancer Center, University of California, San Diego, San Diego, CA
[8] Center for Engineering in Cancer, Institute for Engineering in Medicine, University of California, San Diego, San Diego, CA

*correspondence kbarkovich@health.ucsd.edu and nsteinmetz@ucsd.edu

Abstract

An ongoing challenge in precision medicine is the efficient delivery of therapeutics to tissues/organs of interest. Nanoparticle delivery systems have the potential to overcome traditional limitations of drug and gene delivery through improved pharmacokinetics, tissue targeting, and stability of encapsulated cargo. Physalis mottle virus (PhMV)-like nanoparticles are a promising nanocarrier platform which can be chemically targeted on the exterior and interior surface through reactive amino acids. Cargo-loading to the internal cavity is achieved with thiol-reactive small molecules. However, the internal loading capacity of these nanoparticles is limited by presence of a single reactive cysteine (C75) per coat protein with low inherent reactivity. Here, we use structure-based design to engineer cysteine-added mutants of PhMV VLPs that display increased reactivity towards thiol-reactive small molecules. Specifically, the A31C and S137C mutants show greater than 10-fold increased rate of reactivity towards thiol reactive small molecules and PhMV Cys1 (A31C), PhMV Cys2 (S137C), and PhMV Cys1+2 (double mutant) VLPs display up to three-fold increased internal loading of the small molecule chemotherapeutics aldoxorubicin and vcMMAE and up to four-fold increased internal loading of the MRI imaging reagent DOTA(Gd). These results further improve upon a promising plant virus-based nanocarrier system for use in targeted delivery of small molecule drugs and imaging reagents *in vivo*.

Introduction

There is significant optimism surrounding the use of nanomaterials for the improvement of disease diagnosis and treatment. Specifically, nanoparticles (NPs) have the potential to overcome traditional limitations of drug and gene delivery by improving the stability and pharmacokinetic properties of encapsulated cargo and circumvent biological barriers for targeted delivery.[1,2] Examples of well-studied nanocarrier platforms are reviewed elsewhere,[1] and include lipid-based NPs (e.g. liposomes),[3,4] inorganic NPs (e.g. silica, gold, iron oxide

NPs),[5-7] and polymeric NPs (e.g. dendrimers, co-block polymers)[8] as well protein and virus-based NPs,[9,10] each of which have their own advantages and disadvantages in terms of biocompatibility, pharmacokinetics, and ease of synthesis and small molecule encapsulation.[11] All of these NP systems can be engineered to carry molecular cargo, including chemotherapeutics, immunomodulators, peptide/protein drugs, synthetic nucleic acids, as well as contrast agents.[12] Barriers for the advancement of novel nanomaterials into clinical practice are numerous, and include concerns surrounding reproducible synthesis, scalable manufacturing, toxicity, and poor cargo loading.[13,14]

Virus-based NPs are protein-based nanostructures which make promising nanocarriers based on their high degree of structural uniformity, biocompatibility, and ease of synthesis in biological systems and manipulation by means of chemical conjugation, self-assembly, and genetic engineering.[15] Virus-like particles (VLPs) are proteinaceous NPs derived from the coat proteins (CPs) of viral capsids that lack internal genetic material and are therefore noninfectious.[16] Extensively studied VLPs are derived from the bacteriophages Qβ, P22, and MS2, the mammalian hepatitis B virus (HBV), and plant viruses tobacco mosaic virus (TMV), cowpea chlorotic mottle virus (CCMV), and potato virus X (PVX) – amongst others. These virus-based NPs can be synthesized by recombinant expression of their CPs through fermentation or plant molecular farming and manipulated through chemical biology approaches to carry a diverse array of molecular cargo.[9,16,17] Although noncovalent loading of small molecules does not require modification of the cargo, covalent methods of cargo loading are often preferred as they are less prone to non-specific cargo release.[16] Additionally, the use of enzymatic- or pH-labile linkers, which are widespread in antibody-drug conjugates,[18] can increase specificity of molecular cargo release at the tissue of interest.[19,20]

Our recent interest lies in the development of the VLP platform technology derived from Physalis mottle virus (PhMV). PhMV is a +ssRNA virus from the family *Tymoviridae* that forms a ~30 nm-sized icosahedral capsid from 180 identical CPs, and can be recombinantly expressed and purified as a homogenous and stable VLP.[21] PhMV-based VLPs are an especially promising drug delivery platform due to their long serum half-life ($t_{1/2\ slow}$ ~ 44 hours).[22] The crystal structure of the VLPs has been solved to 3.2 Å, and additional studies have established the inter-subunit ionic interactions that are invariant to mutation in order to maintain viral capsid integrity.[23,24] Previous work established that the PhMV CP can be genetically modified at its N-terminus (which projects internally into the viral particle) with immunogenic peptides,[25,26] and can be chemically modified through a native cysteine (C75) and external lysine residues (K62, K143, K153, and K166).[27] Nevertheless, the PhMV CP offers only a single cysteine residue, therefore the theoretical maximum loading capacity using thiol reactive small molecules is 180 moieties per VLP. Additionally, C75 is somewhat buried in the structure (Figure 1A), restricting accessibility and therefore reactivity.[23,28] To overcome this limitation, we generated a set of cysteine-added mutants of PhMV. We demonstrate that these mutants maintain their structure and display increased reactivity toward thiol-reactive small molecules. We then demonstrate that these mutants increase the internal loading capacity of a variety of chemotherapeutics and imaging small molecules.

Results and Discussion

Preparation and characterization of PhMV VLPs. Our prior work with PhMV VLPs used a gene construct with an N-terminal hexahistadine tag and enterokinase cleavage site (Figure S1A).[27] This form of PhMV VLP is herein referred to as PhMV-HM (HM = Hema Masarapu, who generated and provided this vector). We re-designed the expression system to (1) remove the tag, which is not used for VLP purification and (2) we sought to increase expression yield. We established a dual expression vector system to generate untagged PhMV VLPs (herein referred

to as PhMV-KB) using the carbenicillin-resistance plasmid pRSETa and kanamycin-resistance plasmid pET in *E. coli* (Figure S1). This system improved VLP yield approximately five-fold to ~250 mg of VLP per liter of culture. Approximately 50% of the total bacterial lysate proteins were found to be recombinant PhMV CP (Figure S2A). As expected, SDS-PAGE of PhMV-HM VLPs shows a single band at ~25 kDa corresponding to N-terminal tagged PhMV CP, while PhMV-KB VLPs shows a single band at ~20 kDa, corresponding to the native PhMV CP (Figure S2B). PhMV-HM and PhMV-KB VLP preparations are both monodisperse, homogenous, and have similar whole particle characteristics by native gel electrophoresis, size-exclusion chromatography, dynamic light scattering, and transmission electron microscopy (Figure S2C-F), consistent with prior literature.[21]

Structure-based design of cysteine-added PhMV VLPs. We have previously established that the thiol of the single cysteine (C75) of the PhMV CP, which is oriented internally inside the VLP (Figure 1A), is accessible to alkylation with maleimides under physiologic conditions.[22,27] Despite a theoretical maximum of 180 possible binding sites per VLP, prior studies suggest a maximum of 130-150 maleimide-based small molecules can be bound per VLP using excess small molecules under optimal conditions,[29,30] likely because it is partially buried within the bulk protein (Figure 1B). We hypothesized that further internal-facing amino acids of the PhMV coat protein could be mutated to cysteine to increase the loading capacity of PhMV VLPs without significantly altering the VLP superstructure or changing its surface characteristics. As such, we identified alanine-31 and serine-137 as two potential residues, since both side chains are surface exposed and project internally, and do not participate in the electrostatic interactions between coat proteins that maintain PhMV coat integrity.[28] Additionally, the alpha carbon (Cα) for both amino acids is located greater than 12 Å from C75 and each other (Figure 1C), so are unlikely to form intramolecular disulfide bridges, which are rarely observed with Cα distances

beyond 7.0 Å. [31] Structural modeling of the A31C and S137C mutants predicts these side chains will be highly solvent exposed, and therefore highly accessible to chemical modification (Figure 1D-E).

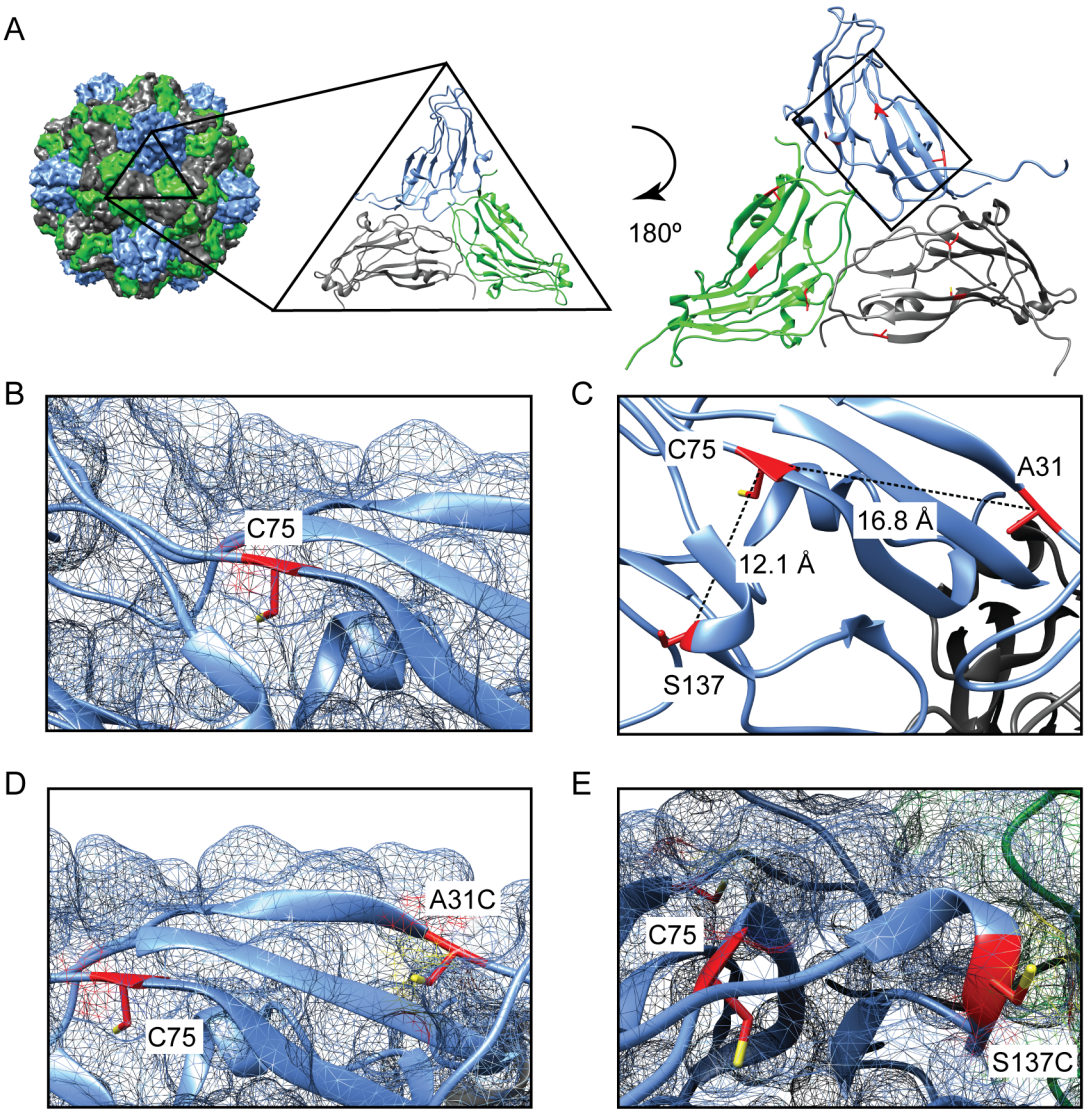

Figure 1. Structure-based design of cysteine-added PhMV VLPs. A. PhMV VLPs (PDB 1QJZ) are composed of 180 identical coat proteins, which are arranged in asymmetric trimers (colored blue, green, grey). Cysteine-75 (C75) is located on the internal coat protein surface, along with A31 and S137 (red). The box surrounds the A chain of the asymmetric unit. B. The side chain of C75 is oriented internally into the bulk protein. The internal-facing protein surface is displayed in mesh. C. Distances of the alpha carbons (Cα) of A31 and S137, relative to the Cα of C75. D-E. Predicted orientation of the side chains of A31C and S137C mutants of PhMV CP.

Plasmids encoding the cysteine-added mutant PhMV CPs were generated through site directed mutagenesis and PhMV Cys1 (A31C), PhMV Cys2 (S137C), and PhMV Cys1+2 (A31C S137C) VLPs were expressed and purified similarly to PhMV VLPs. Cysteine-added CPs had similar migratory characteristics to the native CP on SDS-PAGE (Figure 2A). It should be noted that the VLPs, while devoid of genomic RNA, carry host RNA and differences in RNA affinity was noted. PhMV-KB and PhMV Cys1 VLPs showed similar RNA binding and migration by native gel electrophoresis, while the PhMV Cys2 and PhMV Cys1+2 VLPs shows mildly increased migration toward the cathode (Figure 2B). PhMV Cys1+2 shows reduced RNA carrying, suggestive of reduced RNA affinity. The A260/A280 ratio of PhMV Cys1 is 1.42, nearly identical to that of native PhMV (1.41), while PhMV Cys2 and PhMV Cys1+2 have an A260/A280 of 1.23 and 0.96, respectively, again suggestive of reduced RNA carrying. We hypothesize that the reduced RNA-binding affinity of the PhMV Cys2 and Cys1+2 mutants is due to disruption of native CP-RNA interactions. All PhMV VLPs showed similar elution profiles on size exclusion chromatography, indicating the formation of intact VLPs, and notably without significant free coat protein or evidence of aggregation (Figure 2C). All VLPs were homogenous by dynamic light scattering and showed characteristic ~30 nm diameter on transmission electron microscopy (Figure 2D-E).

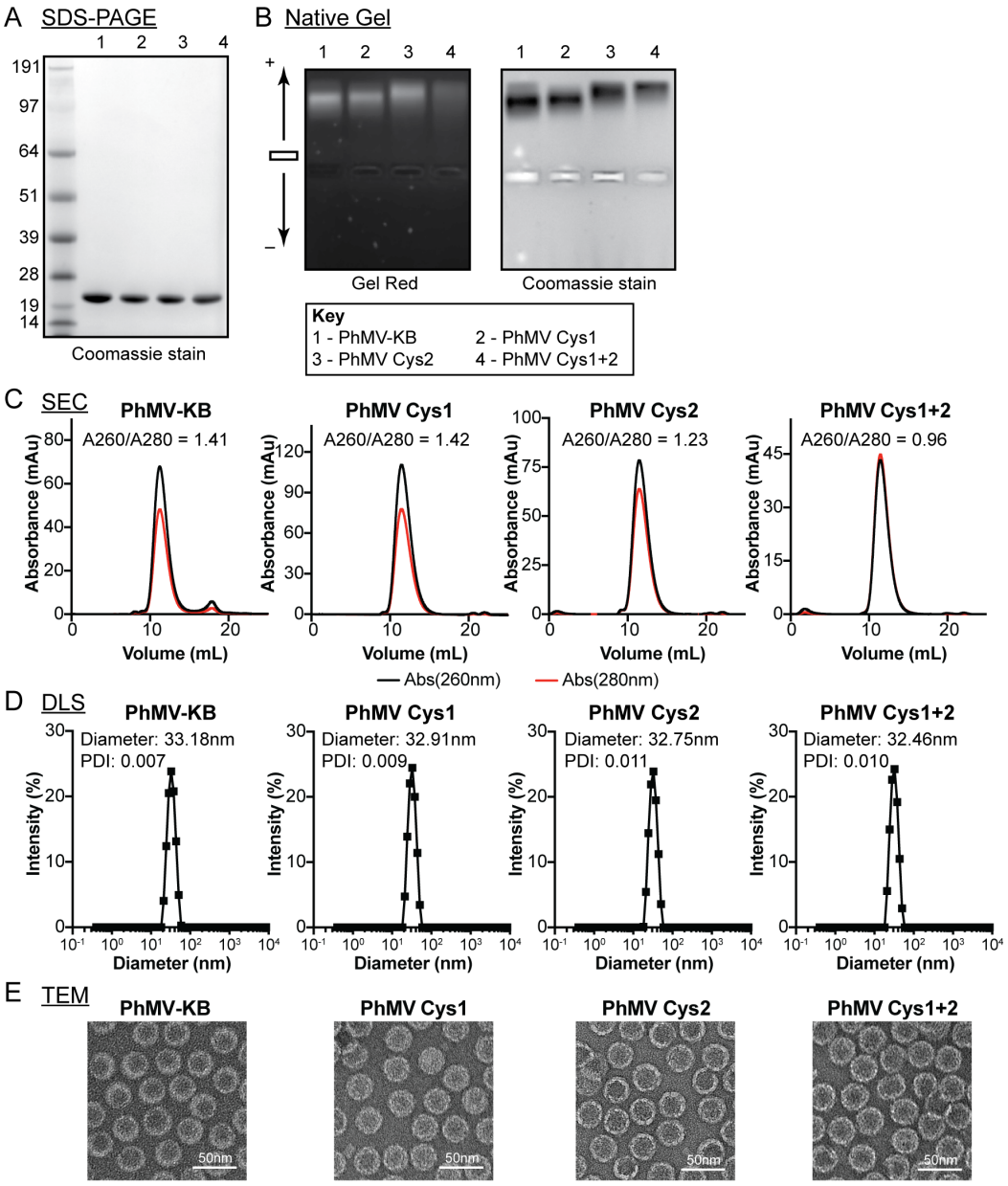

Figure 2. Purification of cysteine-added PhMV VLPs. A-D. Characterization of PhMV-KB, PhMV Cys1, PhMV Cys2, and PhMV Cys1+2 VLPs using SDS-PAGE (A), native gel electrophoresis (B), size-exclusion chromatography (C), dynamic-light scattering (D), and transmission electron microscopy (E). Error bars represent the S.E.M. of five replicates.

Characterization of the cysteine reactivity of cysteine-added PhMV VLPs. We next quantified the concentration of free thiols in PhMV-KB and cysteine-added mutant VLPs using DTNB (5,5'-dithio-bis-(2-nitrobenzoic acid), known as Ellman's reagent), which reacts quickly with free thiols to generate the fluorescent species 5-thio-2-nitrobenzoic acid, which is highly

colored and can be assayed by UV-Vis spectrophotometer at 412 nm and quantified by comparison to a standard curve generated with L-cysteine (Figure 3A). We observed a greater than 10-fold increase in the concentration of free thiols in PhMV VLP cysteine mutants as compared to PhMV-KB (Figure 3B). This difference was substantially decreased after denaturation of the VLPs with SDS (Figure 3C), suggesting the differences in DTNB-reactivity between the native C75 of PhMV and mutant C31 and C137 was due to differences in solvent exposure and/or local environment, which can dramatically alter cysteine pK_a and therefore reactivity,[32] and not due to differences in oxidation.

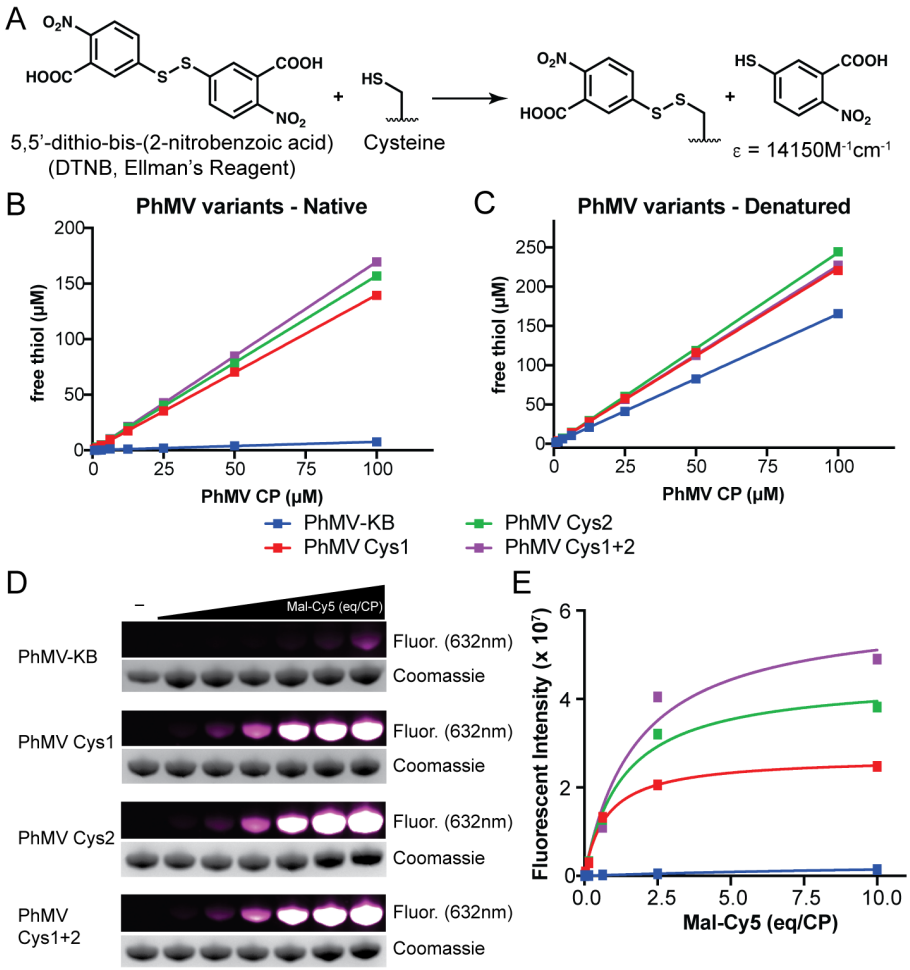

Figure 3. Cysteine-added PhMV VLPs show increased reactivity to thiol reactive small molecules. A. DTNB (5,5'-dithio-bis-(2-nitrobenzoic acid) reacts with reduced cysteines to release 5-thio-2-nitrobenzoic acid, which is highly absorbent at 412 nm. B-C. Quantification of free thiol concentration of native (B) or chemically denatured (C) PhMV-KB or cysteine-added VLPs using DTNB. D-E. Incubation of PhMV-KB or cysteine-added VLPs with maleimide-Cy5 followed by separation by SDS-PAGE (D) and quantification of in gel fluorescence (E).

154

155 We next assessed the reactivity of PhMV-KB and cysteine mutant VLPs to maleimide-Cy5.
156 Maleimides are commonly used thiol-reactive warheads for the bioconjugation of small
157 molecules to macromolecules. While we typically perform bioconjugation reactions between the
158 native cysteines of PhMV VLPs and maleimide-containing small molecules for at least 16 hours
159 to increase modification efficiency, we performed this experiment for only 6 hours to maximize
160 potential differences in reactivity between PhMV-KB and the Cys1, Cys2, and Cys1+2 mutants.
161 After reactions were quenched, VLPs were denatured and separated by SDS-PAGE to avoid

potential internal fluorescent quenching within the VLP.[27] We observed a marked difference in the amount of modification of native PhMV coat proteins as compared to cysteine-added mutants, as indicated by markedly increased fluorescent signal (Figure 3D). Quantitatively, PhMV Cys1, PhMV Cys2, and PhMV Cys1+2 CPs showed 17-, 26-, and 34-fold increased fluorescent labeling, respectively, as compared to PhMV-KB (Figure 3E), consistent with results with DTNB. Overall, these results indicate that the Cys1, Cys2, and Cys1+2 mutants of PhMV have markedly increased reactivity to cysteine-reactive small molecules.

Characterization of the aldoxorubicin loading capacity of cysteine-added PhMV VLPs. We have previously shown that the chemotherapeutic doxorubicin can be chemically conjugated to PhMV VLPs through reaction with aldoxorubicin,[30] which contains a cysteine-reactive maleimide coupled to doxorubicin through an acid-labile hydrazone linker (Figure 4A). [19] Doxorubicin remains covalently associated with these VLPs at physiologic pH but is released in the acidic tumor microenvironment or after endocytosis into the acidic endolysosomal compartment. [33] We purified aldoxorubicin-conjugated PhMV-KB and cysteine mutants, PhMV-KB-Aldox, PhMV Cys1-Aldox, PhMV Cys2-Aldox, and PhMV Cys1+2-Aldox, and ensured removal of excess small molecules by ultracentrifugation over a sucrose cushion. As expected, we observed covalent modification of native PhMV and cysteine-added CPs with aldoxorubicin, as illustrated by increased coat protein fluorescence at 488 nm (Figure 4B). All aldoxorubicin-conjugated VLPs maintained structural integrity and were homogenous and monodisperse (Figure S3A-B). The amount of covalently bound doxorubicin, as measured by UV-Vis spectrometry, was significantly increased in all cysteine mutant VLPs as compared to PhMV-KB; the average number of doxorubicin molecules per VLP was 83, 184, 235, and 238 for PhMV-KB-Aldox, PhMV Cys1-Aldox, PhMV Cys2-Aldox, and PhMV Cys1+2-Aldox, respectively (Figure 4C-D). To assess if the doxorubicin within these PhMV VLPs remained functional, we determined the cytotoxicity for each VLP in A2780 ovarian cancer cells. All Aldox-VLPs show dose-dependent

cytotoxicity (Figure 4E). PhMV Cys2-Aldox and PhMV Cys1+2-Aldox had significantly decreased IC50 values of 11.2 μg/mL and 9.88 μg/mL, respectively, as compared to PhMV-KB-Aldox, which had an IC50 of 36.8 μg/mL (Figure 4F). When normalized to the delivered aldoxorubicin concentration, there is no significant difference in cytotoxicity between aldoxorubicin-conjugated PhMV VLPs (Figure S3C-D), which suggests that observed differences in cytotoxicity at a given VLP concentration is due to the variation in doxorubicin delivered per VLP, and not an altered mechanism of cytotoxicity upon delivery.

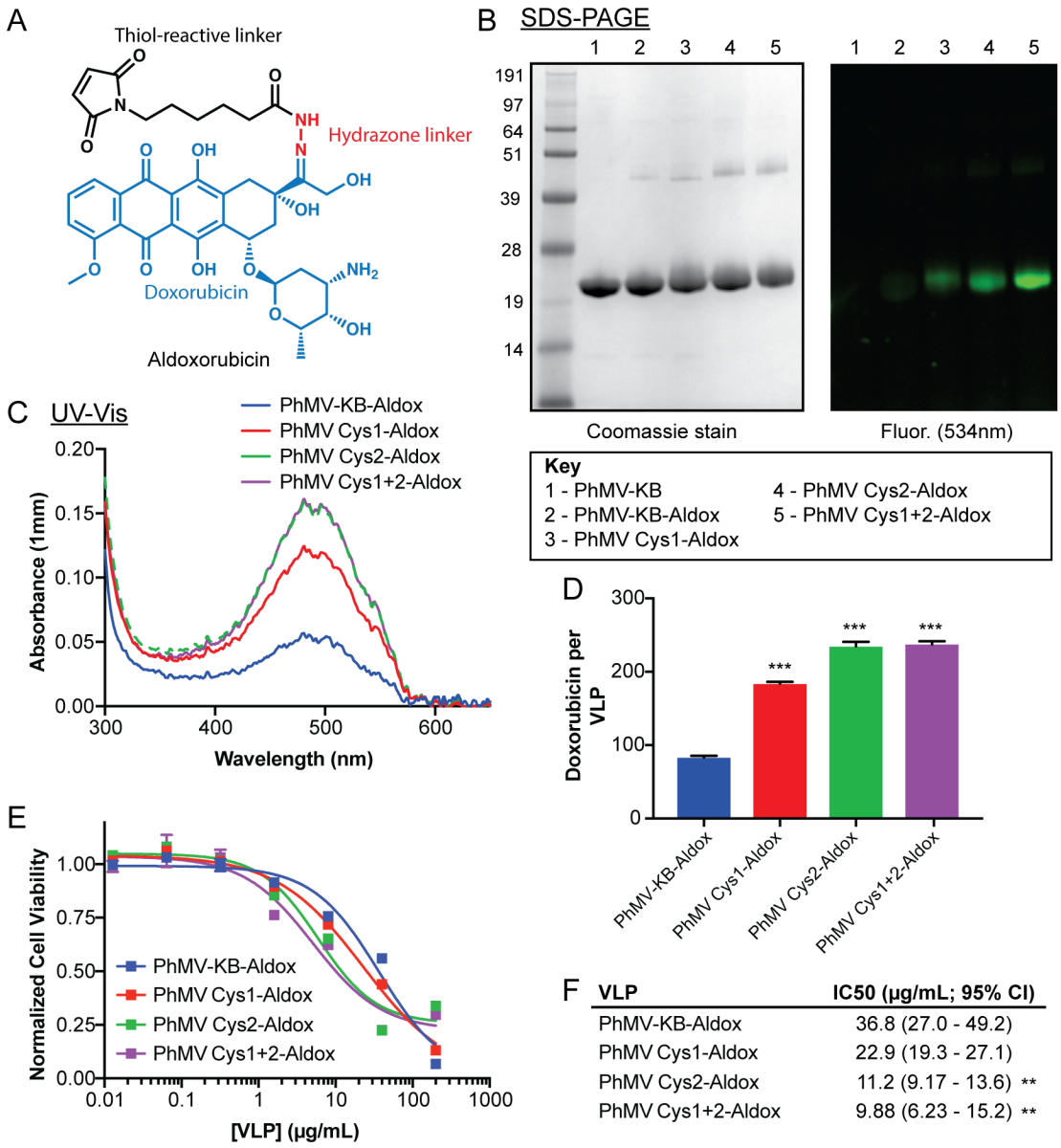

Figure 4. Cysteine-added PhMV VLPs show increased aldoxorubicin loading capacity and resultant NPs display improved cytotoxicity. A. Chemical components of aldoxorubicin. B-C. Characterization of PhMV-KB-Aldox, PhMV Cys1-Aldox, PhMV Cys2-Aldox, and PhMV Cys1+2-Aldox VLPs by SDS-PAGE (B) and UV-Vis spectroscopy (C). D. Calculation of doxorubicin per VLP based on particle absorbance at 480 nm. E-F. Dose-response curve (E) and calculated IC50 (F) of Aldox-conjugated PhMV VLPs in A2780 cells. Error bars represent the S.E.M. of three replicates (some error bars are smaller than the data point symbol). **: p<0.01, ***: p<0.001.

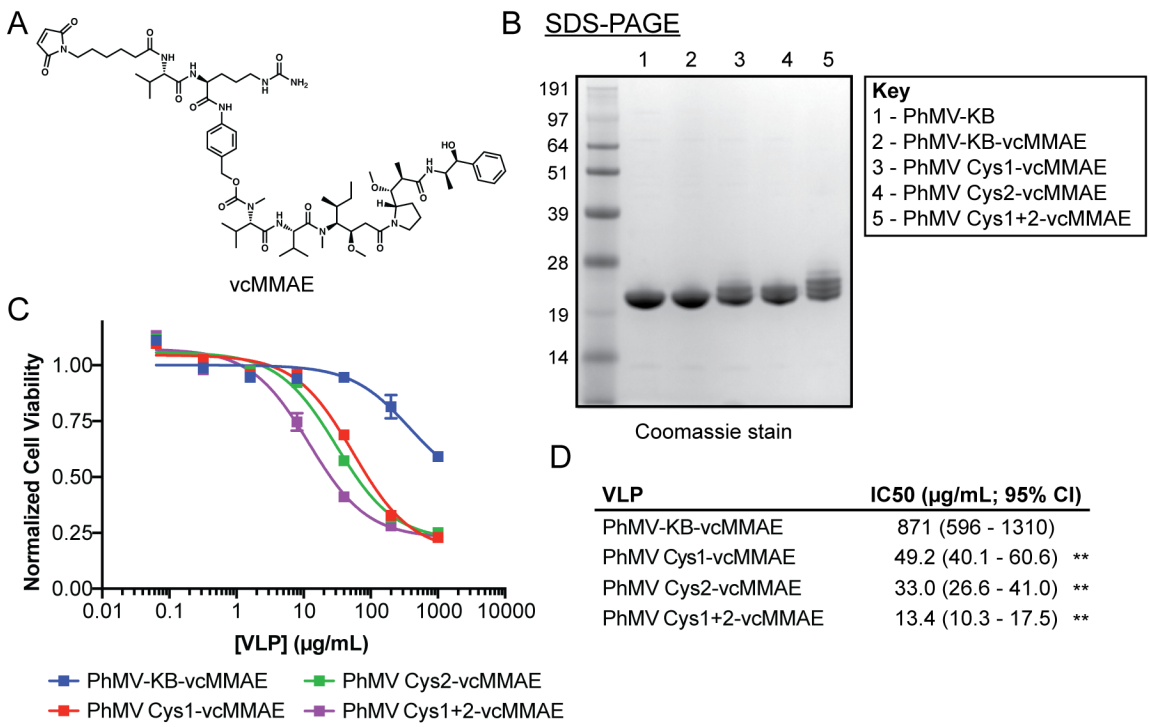

Figure 5. Cysteine-added PhMV VLPs show increased vcMMAE loading capacity and resultant NPs display improved cytotoxicity. A. Chemical structure of valine-citrulline monomethyl auristatin E (vcMMAE). B. Characterization of PhMV-KB-vcMMAE, PhMV Cys1-vcMMAE, PhMV Cys2-vcMMAE, and PhMV Cys1+2-vcMMAE VLPs by SDS-PAGE. C-D. Dose-response curve (C) and calculated IC50 (D) of vcMMAE-conjugated PhMV VLPs in A2780 cells. Error bars represent the S.E.M. of three replicates (some error bars are smaller than the data point symbol). **: p<0.01.

Characterization of the MMAE loading capacity of cysteine-added PhMV VLPs.

Monomethyl auristatin E (MMAE), a derivative of the anti-tubulin cytotoxin auristatin E,[34] is widely used in antibody drug conjugates. It is often conjugated to tumor-targeting antibodies as vcMMAE which contains a reactive maleimide and a valine-citrulline (vc) linker (Figure 5A), which highly stable in serum but is rapidly cleaved in the endolysosomal compartment to expose the toxic payload.[20] We have previously shown that vcMMAE can be chemically conjugated to the native cysteines of the PVX and engineered thiols of TMV for tumor delivery.[35,36] We purified vcMMAE-conjugated PhMV-KB and cysteine-added mutants, PhMV-KB-vcMMAE, PhMV Cys1-vcMMAE, PhMV Cys2-vcMMAE, and PhMV Cys1+2-vcMMAE, and ensured removal of excess small molecules by ultracentrifugation over a sucrose cushion. vcMMAE has a molecular weight of 1.3 kDa, so covalent adducts with the PhMV coat protein can be observed by gel shift on

SDS-PAGE. While we observed minimal modification of the native PhMV CP, approximately one-half of the PhMV Cys1 and PhMV Cys2 CPs show bioconjugation to vcMMAE, and greater than two-thirds of the PhMV Cys1+2 CPs are single, doubly, or triply modified (Figure 5B). When quantified by densitometry, this corresponds to approximately 43, 118, 109, and 202 vcMMAE molecules covalently bound to PhMV-KB-vcMMAE, PhMV Cys1-vcMMAE, PhMV Cys2-vcMMAE, and PhMV Cys1+2-vcMMAE VLPs, respectively. All vcMMAE-conjugated VLPs maintained structural integrity and were homogenous and monodisperse (Figure S4A-B). To assess if MMAE bound to PhMV VLPs could be appropriately released for cytotoxic effect, we determined the cytotoxicity for each PhMV-vcMMAE VLP in A2780 cells. All vcMMAE-VLPs show dose dependent cytotoxicity (Figure 5C). PhMV Cys1-vcMMAE, PhMV Cys2-vcMMAE, and PhMV Cys1+2-vcMMAE had significantly decreased IC50 values of 49.2 μg/mL, 33.0 μg/mL, and 13.4 μg/mL, respectively, as compared to PhMV-KB-vcMMAE, which had an IC50 of 871 μg/mL (Figure 5D). When normalized to the delivered vcMMAE concentration, there is a similar trend in cytotoxicity between vcMMAE-conjugated PhMV VLPs (Figure S4C-D), with IC50 values of 1.62 μM, 999 nM, and 754 nM of vcMMAE delivered by PhMV Cys1-vcMMAE, PhMV Cys2-vcMMAE, and PhMV Cys1+2-vcMMAE, respectively, compared to 10.5 μM for PhMV-KB-vcMMAE. This suggests that there may be an additive advantage with delivery of a larger number of vcMMAE molecules per NP.

Characterization of the Gd(III) loading capacity of cysteine-added PhMV VLPs. Gadolinium (Gd), an element of the lanthanide series that is highly paramagnetic due to its seven unpaired electrons, is commonly used as an magnetic resonance imaging (MRI) contrast agent. [37] Owing to its toxicity in a free state, Gd(III) is administered bound to a metal chelate, often diethylenentriamene pentaacetate (DTPA) or 2,2',2'',2'''-(1,4,7,10-tetrazacyclododecane-1,4,7,10-tetrayl)tetraacetic acid (DOTA).[38] We have previously shown that maleimide-functionalized DOTA (Figure 6A) can be conjugated to PhMV VLPs through reactive thiols to

generate a PhMV-based T_1 MR contrast agent.[22] Here we conjugated DOTA in the presence of Gd; we purified DOTA(Gd)-conjugated PhMV-KB and cysteine-added mutants, PhMV-KB-DOTA(Gd), PhMV Cys1-DOTA(Gd), PhMV Cys2-DOTA(Gd), and PhMV Cys1+2-DOTA(Gd), and ensured removal of excess Gd(III) ions by buffer exchange chromatography, ultracentrifugation, and dialysis. Maleimide-DOTA has a molecular weight of 786 Da, so a small gel shift is observed on SDS-PAGE after covalent modification of the PhMV coat protein. It is difficult to quantify DOTA-binding by this method, but PhMV Cys1+2 CPs clearly show a more substantial gel shift than the single mutants PhMV Cys1 and PhMV Cys2, or native PhMV CPs (Figure 6B). All DOTA(Gd)-conjugated VLPs maintained structural integrity and were homogenous and monodisperse (Figure S5A-B). The number of Gd(III) ions per VLP, as measured by ICP-MS, was significantly increased in all cysteine-added PhMV VLPs as compared to PhMV-KB; the average number of Gd(III) ions per VLP was 26.8, 52.6, and 87.7 for PhMV Cys1-DOTA(Gd), PhMV Cys2-DOTA(Gd), and PhMV Cys1+2-DOTA(Gd), respectively, compared to 19.1 for PhMV-DOTA(Gd) (Figure 6C). Future studies exploring preformation and purification of the Mal-DOTA(Gd) complex prior to reaction with PhMV VLPs could be performed to further optimize Gd-loading efficiency.

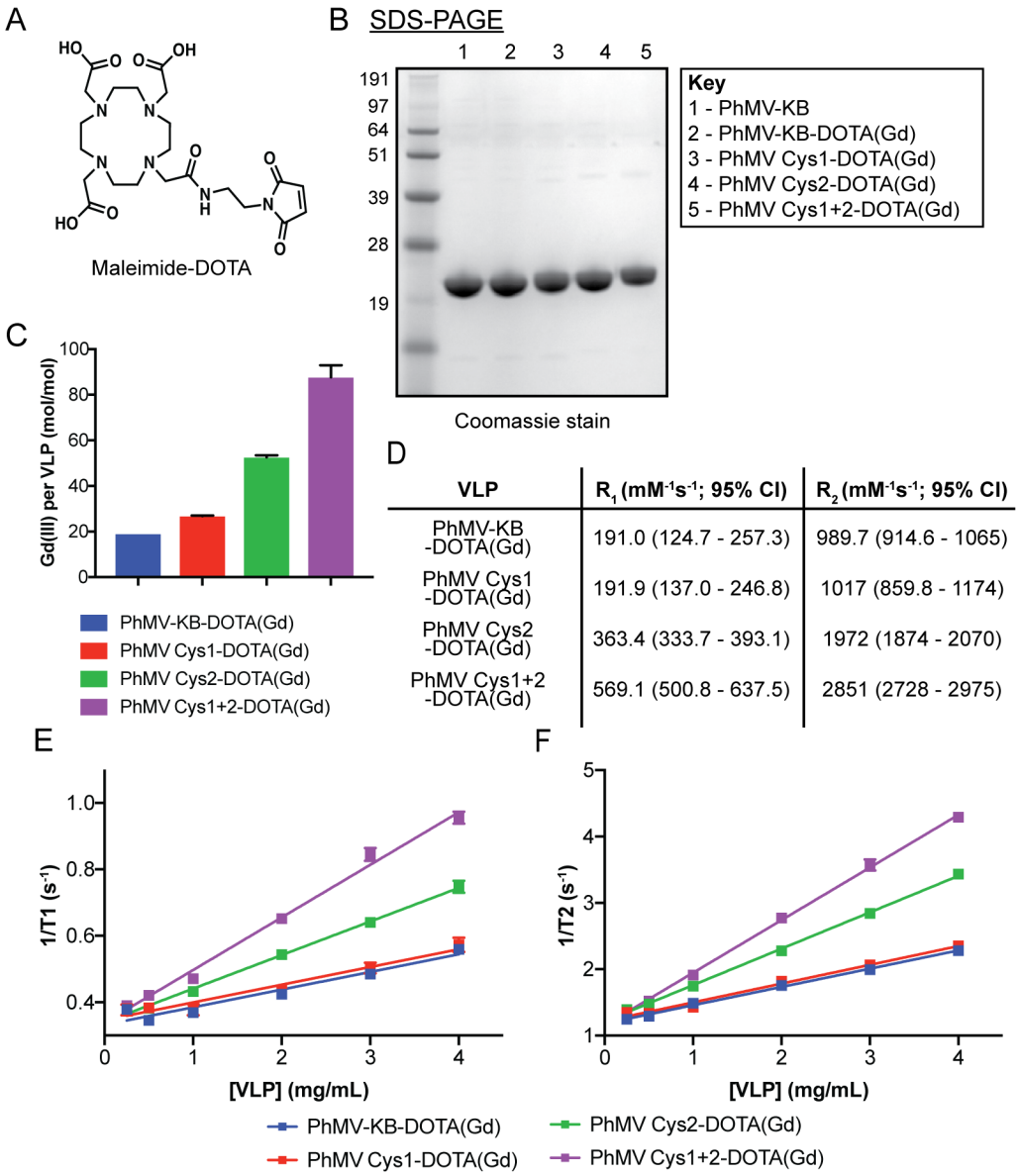

Figure 6. Cysteine-added PhMV VLPs show increased DOTA(Gd) loading capacity and resultant NPs display high R_1 and R_2 relaxivities. A. Chemical structure of the gadolinium chelate maleimide-DOTA. B. Characterization of PhMV-KB-DOTA(Gd), PhMV Cys1-DOTA(Gd), PhMV Cys2-DOTA(Gd), and PhMV Cys1+2-DOTA(Gd) VLPs by SDS-PAGE. C. Calculation of number of Gd(III) ions per VLP based on ICP-MS data. D-F. Summary data (D) and curves of longitudinal (R_1) (E) and transverse (R_2) (F) relaxivities of PhMV-KB-DOTA(Gd), PhMV Cys1-DOTA(Gd), PhMV Cys2-DOTA(Gd), and PhMV Cys1+2-DOTA(Gd) VLPs at room temperature in a 3 T MR scanner.

250

251 To assess if the increased Gd(III) ion loading translated to improved T_1-weighted MR contrast

252 attributes, we next determined the T_1 and T_2 of a concentration series of the DOTA(Gd)-

253 conjugated VLPs at 3.0 T (Supplemental Figure 6A). Owing to their similar Gd(III) ion loading,

the R_1 and R_2 of PhMV-KB-DOTA(Gd) and PhMV Cys1-DOTA(Gd) were not significantly different, whereas PhMV Cys2-DOTA(Gd) and PhMV Cys1+2-DOTA(Gd) showed 1.90 and 2.98-fold increased R_1 values, respectively (Figure 6D-F), indicated improved T_1-weighted MR signal per VLP. The relatively high R_2/R_1 ratio of these VLPs (~5.0) is expected based on the high magnetic field strength used for these experiments, but suggests that further optimization of Gd(III) loading may be required to maximize their T_1-weighted MR signal.[39] R_1-relaxivity is also typically determined per Gd(III) ion to allow for comparison across monomeric vs multivalent systems,[40] and was calculated for all DOTA(Gd)-conjugated PhMV VLPs (Supplemental Figure 6B-D). The r_1 of PhMV-KB-DOTA(Gd) was 10.0 $mM^{-1}s^{-1}$ per Gd(III) ion, consistent with MR theory and prior results that high molecular weight complexes show increased r_1-relaxivity due to slowed molecular tumbling (τ_R).[37,41] The DOTA(Gd)-conjugated PhMV cysteine mutants displayed decreased r_1 of 7.17 $mM^{-1}s^{-1}$, 6.91 $mM^{-1}s^{-1}$, and 6.49 $mM^{-1}s^{-1}$ per Gd(III) for PhMV Cys1-DOTA(Gd), PhMV Cys2-DOTA(Gd), and PhMV Cys1+2-DOTA(Gd), respectively. Since no difference in total internal hydration is expected across these different VLPs, this observation may be due to increased water residency time (τ_m) (i.e., decreased rates of exchange of inner shell and bulk water molecules) in PhMV VLPs with higher total Gd(III) ion count or increased coordination of other ligands such as phosphate or endogenous RNA.[41] Nevertheless, these results demonstrate that the increased Gd(III) ion loading capacity of cysteine-added PhMV VLPs correlate with overall improved T_1-MR contrast agent properties.

Conclusions

We have used structure-based design to rationally design a series of cysteine-added mutants of PhMV VLPs to increase the internal covalent loading capacity. We show that these mutants show increased reactivity towards thiol-reactive small molecules, including the chemotherapeutics aldoxorubicin and vcMMAE, and the MRI contrast agent DOTA(Gd). These

cysteine-added mutants improve upon the PhMV VLP technology, which shows promise as a platform for the targeted delivery of small molecule drugs and imaging reagents *in vivo*.

Methods

Preparation of PhMV VLPs and cysteine-added mutants. PhMV-HM VLPs were prepared by expressing the CP in BL21(DE3), as previously described.[27] To prepare native PhMV VLPs (referred to as PhMV-KB VLPs), the PhMV CP gene (NCBI Gene ID 940246) was cloned into pRSETa and pET vectors using established methods (Figure S1).[42] PhMV VLPs were then expressed in BL21(DE3) with minimal modifications to the method previous described.[21,27] The key difference between PhMV-HM and PhMV-KB is that the HM expression construct introduces a cleavable N-terminal hexahistadine tag, while PhMV-KB does not (HM = Hema Masarapu, who generated and provided this vector). Briefly, BL21(DE3) were double transformed with pRSETa-PhMV CP (carbenicillin resistant) and pET-PhMV CP (kanamycin resistant) to increase the plasmid copy number per cell. A single colony was isolated and used to inoculate 50 mL of Luria Broth (LB, Sigma) supplemented with carbenicillin at 50 µg/mL and kanamycin at 50 µg/mL, which was grown for 18 hours at 37 ºC. This was used at a 1:100 dilution to inoculate 1 L of terrific broth (TB, Sigma Aldrich) supplemented with carbenicillin and kanamycin. Cultures were grown to OD_{600} ~ 1.0 and induced with 0.5 mM IPTG (Sigma) at 30 ºC overnight. Cultures were then pelleted at 7,500 x g for 10 min at 4 ºC, lysed by sonication in 50 mM sodium citrate pH 5.5 (SCB) and clarified at 30,000 x g for 30 min at 4 ºC. Lysates were then ultracentrifuged at an average of 111,818 x g for 3 hours at 4 ºC. Pellets were resuspended overnight in SCB and extracted with 0.5 volumes of 1:1 n-BuOH:$CHCl_3$. The aqueous layer was isolated, layered onto a 10-40% linear sucrose gradient and separated by ultracentrifugation at an average of 103,613 x g for 3 hours at 4 ºC. The light scattering zone was collected, diluted with SCB, and centrifuged at an average of 161,018 x g for 3 hours at 4 ºC. The final pellet was resuspended in SCB supplemented with 0.5 mM TCEP (Sigma Aldrich)

to yield pure VLPs, which were concentrated to greater than 10 mg/mL and stored at 4 ºC. Protein concentration was determined by BCA Assay (Thermo Fisher) using bovine serum albumin (BSA) as a standard. Yields were typically 250 mg of VLP per 1 L of bacterial culture. Plasmids for the expression of cysteine-added mutants of PhMV (PhMV Cys1 (A31C), PhMV Cys2 (S137C), PhMV Cys3 (A31C S137C)) were generated by polymerase chain reaction (PCR)-based site-directed mutagenesis using a high-fidelity polymerase (Q5, New England Biolabs [NEB]), and the mutagenesis primers listed in Supplemental Table 1. Crude PCR reactions were digested with Dpn-I (NEB), purified to remove free nucleotides, and used to transform DH5α (NEB). Single colonies were isolated and amplified and vector integrity was confirmed by DNA sequencing. PhMV Cys1, PhMV Cys2, and PhMV Cys1+2 VLPs were purified similarly to PhMV-KB VLPs.

VLP characterization. VLPs were characterized by SDS-PAGE (5 µg VLP on a 12% Bis-Tris, NuPAGE, Thermo Fisher), native gel electrophoresis (10 µg VLP on a 0.8% agarose in TBE), UV-Vis (Nanodrop 200 spectrophotometer, ThermoFisher), size exclusion (Superose 6 Increase 10/300 GL column at 0.5 mL/min on an AKTA FPLC, GE), dynamic light scattering (Zetasizer Nano ZSP/Sen5600, Malvern Panalytical), and transmission electron microscopy with 400-mesh hexagonal copper grids using UAc-negative-staining (2% w/v) and a FEI TecnaiSpirit G2 BioTWIN TEM at 80 kV for image acquisition, as applicable. The concentration of PhMV-bound doxorubicin was determined by UV-Vis spectroscopy using the extinction coefficient ε(DOX, 488 nm) = 11,500 $M^{-1}cm^{-1}$. The concentration of Gd(III) ions was determined by inductively coupled plasma-mass spectrometry (ICP-MS). Briefly, 10 µL of sample was diluted in 490 µL concentrated nitric acid and 500 µL distilled water. The sample was then heated to 95 ºC for 10 min then added to 9 mL distilled water prior to analysis using an iCAP RQ system (Thermo

Fisher). Samples were compared to four standard concentrations of Gd(III) (Sigma-Aldrich). All measurements were completed in duplicate.

Structural analysis. Structural analysis of PhMV VLPs was performed using UCSF Chimera[43] using datasets PDB 1QJZ and PDB 1E57. The Multiscale models function was used for generation of the complete VLP. Modeling of cysteine-added mutants was performed with the rotamers tool using the Dunbrack 2010 rotamer library,[44] selecting the highest probability cysteine rotamer.

Cysteine reactivity studies using DTNB and maleimide-Cy5. Free thiol concentrations of PhMV-KB and cysteine-added mutant VLPs were determined using DTNB (5,5'-dithio-bis-(2-nitrobenzoic acid), Ellman's reagent, Thermo Fisher). Serial dilutions of PhMV-KB or cysteine-added mutant VLPs (100 μM -> 0.78 μM CP) were made in 10 mM KP pH 8.0. DTNB was then added to a final concentration of 200 μM and the reaction mixture was incubated at room temperature for 15 minutes. The resulting solution was then analyzed on a plate reader (Tecan) for absorbance at 412 nm. Free thiol concentrations were determined by comparison with a standard curve generated using L-cysteine (Sigma Aldrich). Denaturation studies were performed by heating of VLPs at 95 ºC for 5 min in 1% sodium dodecyl sulfate (SDS, Sigma-Aldrich), followed by serial dilution, reaction with DTNB, and analysis on a plate reader, as above.

PhMV-KB or cysteine-added mutant VLPs were incubated with serial dilutions of maleimide-sulfoCy5 (10 eq/CP -> 0.01 eq/CP; LumiProbe) in 10 mM KP pH 7.5 at room temperature for 6 hours. Samples were then quenched with 50 mM dithiothreitol (DTT, Gold Bio), denatured at 95ºC in SDS-loading buffer and separated by SDS-PAGE. In-gel fluorescence was measured

using a FluorChem R system (ProteinSimple), then gels were stained with Coomassie Blue. Quantification was performed using FIJI (NIH).[45]

Bioconjugation reactions with active ingredients. PhMV-KB or cysteine-added mutant VLPs were incubated with aldoxorubicin (MedChem Express) or valine-citrulline monomethyl auristatin E (vcMMAE; MedChem Express) at 3 molar equivalents per CP (eq/CP) in 10 mM potassium phosphate (KP) pH 7.5, overnight at room temperature. The resulting product was purified by ultracentrifugation (121,139 x g, 70 min) over a sucrose cushion (20% sucrose). The pellet was resuspended in PBS and resulting drug-laden VLPs were concentrated to 5-10 mg/mL and stored at 4ºC. DOTA(Gd)-conjugated PhMV VLPs were generated by incubation of PhMV-KB or cysteine-added mutant VLPs with 3 eq/CP 1,4,7,10-Tetraazacyclododecane-1,4,7-tris-acetic acid-10-maleimidoethylacetamide (Mal-DOTA, Macrocyclics) and 10 eq/CP $GdCl_3$ in TBS (25 mM Tris pH 7.5, 150 mM NaCl) at room temperature overnight. VLPs were then purified by buffer exchange (PD-10 column), ultracentrifugation, as above, and dialyzed into PBS to remove unbound Gd(III). Final DOTA(Gd)-laden VLPs were concentrated to 5-10 mg/mL and stored at 4 ºC.

Cytotoxicity assay. A2780 cells were cultured in RPMI media (Corning) supplemented with 10% fetal bovine serum (FBS, R&D Systems) and 1% penicillin-streptomycin (Cytiva) at 37ºC in a 5% CO_2 humidified incubator. A2780 cells were plated at 3,000 cells/well in 96 well plates and grown overnight. Serial dilutions of Aldox- or vcMMAE-conjugated PhMV VLPs were added directly to the media and cells were incubated for an additional 72 hours. Cells were then analyzed using a CellTiter Glo assay (Promega) according to the manufacture's protocol. All conditions were performed in triplicate. Curves were fit using a least-squares methods (Prism, GraphPad).

MR relaxivity studies. The magnetic resonance transverse and longitudinal relaxivities of DOTA(Gd)-conjugated PhMV-KB and cysteine-added mutant VLPs were determined on a preclinical 3.0 T scanner (BioSpec 3T, Bruker) using an 82 mm inner diameter transmit-receive volume coil. T1 mapping was performed using a variable repetition time (TR) rapid acquisition with relaxation enhancement (RARE) sequence with 10 TRs ranging from 390 – 6990 ms and echo time (TE) 7 ms. T2 mapping was performed using a Carr-Purcell-Meiboom-Gill (CPMG) sequence with TR 9853 ms and 20 TEs ranging from 30-600 ms. T1 and T2 values were calculated using the Image Sequence Analysis tool on ParaVision 360 v3.3 (Bruker) and values plotted using Prism (GraphPad). R_1 and R_2 were calculated using a linear fit (least-squares).

Author Contributions

K.J.B., Z.W., Z.Z., A.S., and E.Y.C. performed experiments. K.J.B., E.Y.C., and N.F.S. designed and analyzed experiments. K.J.B. and N.F.S. wrote the manuscript.

Conflict of Interest

Dr. Steinmetz is a co-founder of, has equity in, and has a financial interest with Mosaic ImmunoEnginering Inc. Dr. Steinmetz serves as Director, Board Member, and Acting Chief Scientific Officer, and paid consultant to Mosaic. The other authors declare no potential COI.

Acknowledgements and Funding

This work was funded in part by the National Institutes of Health (NIH T32EB005970, to UCSD Dept. of Radiology; R01-CA202814 and R01-CA253615, to N.F.S.), the Shaughnessy Family Fund to the Center for Nano-ImmunoEngineering, Department of Veterans Affairs, Veterans Health Administration, Office of Research and Development (I01CX001388 and I01BX005952, to E.Y.C.), and RSNA Research & Education Foundation (RR2251, to K.J.B.). The views expressed in this article are those of the authors and do not necessarily reflect the position or

policy of the Department of Veterans Affairs or the United States government. The content is solely the responsibility of the authors and does not necessarily represent the official views of the RSNA R&E Foundation. Molecular graphics and analyses performed with UCSF Chimera, developed by the Resource for Biocomputing, Visualization, and Informatics at the University of California, San Francisco, with support from NIH P41-GM103311. We thank all members of the Steinmetz lab for helpful discussions and critical review.

References

(1) Mitchell, M. J., Billingsley, M. M., Haley, R. M., Wechsler, M. E., Peppas, N. A., and Langer, R. (2021) Engineering precision nanoparticles for drug delivery. *Nat Rev Drug Discov 20*, 101–124.
(2) Blanco, E., Shen, H., and Ferrari, M. (2015) Principles of nanoparticle design for overcoming biological barriers to drug delivery. *Nat. Biotechnol. 33*, 941–951.
(3) Kabil, M. F., Badary, O. A., Bier, F., Mousa, S. A., and El-Sherbiny, I. M. (2023) A comprehensive review on lipid nanocarrier systems for cancer treatment: fabrication, future prospects and clinical trials. *J Liposome Res* 1–43.
(4) Hou, X., Zaks, T., Langer, R., and Dong, Y. (2021) Lipid nanoparticles for mRNA delivery. *Nat Rev Mater 6*, 1078–1094.
(5) Liang, R., Wei, M., Evans, D. G., and Duan, X. (2014) Inorganic nanomaterials for bioimaging, targeted drug delivery and therapeutics. *Chem Commun 50*, 14071–14081.
(6) Baeza, A., Ruiz-Molina, D., and Vallet-Regí, M. (2017) Recent advances in porous nanoparticles for drug delivery in antitumoral applications: inorganic nanoparticles and nanoscale metal-organic frameworks. *Expert Opin Drug Deliv 14*, 783–796.
(7) Samrot, A. V., Sahithya, C. S., A, J. S., Purayil, S. K., and Ponnaiah, P. (2021) A review on synthesis, characterization and potential biological applications of superparamagnetic iron oxide nanoparticles. *Current Research in Green and Sustainable Chemistry 4*, 100042.
(8) Sung, Y. K., and Kim, S. W. (2020) Recent advances in polymeric drug delivery systems. *Biomater Res 24*, 12–12.
(9) Ma, Y., Nolte, R. J. M., and Cornelissen, J. J. L. M. (2012) Virus-based nanocarriers for drug delivery. *Adv Drug Deliv Rev 64*, 811–825.
(10) Jeevanandam, J., Pal, K., and Danquah, M. K. (2019) Virus-like nanoparticles as a novel delivery tool in gene therapy. *Biochimie 157*, 38–47.
(11) Wilhelm, S., Tavares, A. J., Dai, Q., Ohta, S., Audet, J., Dvorak, H. F., and Chan, W. C. W. (2016) Analysis of nanoparticle delivery to tumours. *Nat Rev Mater 1*, 16014.
(12) Caster, J. M., Patel, A. N., Zhang, T., and Wang, A. (2017) Investigational nanomedicines in 2016: a review of nanotherapeutics currently undergoing clinical trials. *Wiley Interdiscip Rev Nanomed Nanobiotechnol 9*, e1416.
(13) Shi, J., Kantoff, P. W., Wooster, R., and Farokhzad, O. C. (2017) Cancer nanomedicine: progress, challenges and opportunities. *Nat. Rev. Cancer 17*, 20–37.
(14) Liu, Y., Yang, G., Jin, S., Xu, L., and Zhao, C.-X. (2020) Development of High-Drug-Loading Nanoparticles. *Chempluschem 85*, 2143–2157.
(15) Steinmetz, N. F. (2010) Viral nanoparticles as platforms for next-generation therapeutics and imaging devices. *Nanomedicine: Nanotechnology, Biology, and Medicine 6*, 634–641.
(16) Rohovie, M. J., Nagasawa, M., and Swartz, J. R. (2017) Virus-like particles: Next-generation nanoparticles for targeted therapeutic delivery. *Bioeng Transl Med 2*, 43–57.

(17) Wijesundara, Y. H., Herbert, F. C., Kumari, S., Howlett, T., Koirala, S., Trashi, O., Trashi, I., Al-Kharji, N. M., and Gassensmith, J. J. (2022) Rip it, stitch it, click it: A Chemist's guide to VLP manipulation. *Virology 577*, 105–123.
(18) McCombs, J. R., and Owen, S. C. (2015) Antibody drug conjugates: design and selection of linker, payload and conjugation chemistry. *AAPS J 17*, 339–351.
(19) Lebrecht, D., Geist, A., Ketelsen, U.-P., Haberstroh, J., Setzer, B., Kratz, F., and Walker, U. A. (2007) The 6-maleimidocaproyl hydrazone derivative of doxorubicin (DOXO-EMCH) is superior to free doxorubicin with respect to cardiotoxicity and mitochondrial damage. *Int J Cancer 120*, 927–934.
(20) Francisco, J. A., Cerveny, C. G., Meyer, D. L., Mixan, B. J., Klussman, K., Chace, D. F., Rejniak, S. X., Gordon, K. A., DeBlanc, R., Toki, B. E., Law, C.-L., Doronina, S. O., Siegall, C. B., Senter, P. D., and Wahl, A. F. (2003) cAC10-vcMMAE, an anti-CD30-monomethyl auristatin E conjugate with potent and selective antitumor activity. *Blood 102*, 1458–1465.
(21) Sastri, M., Kekuda, R., Gopinath, K., Kumar, C. T., Jagath, J. R., and Savithri, H. S. (1997) Assembly of physalis mottle virus capsid protein in Escherichia coli and the role of amino and carboxy termini in the formation of the icosahedral particles. *J. Mol. Biol. 272*, 541–552.
(22) Hu, H., Masarapu, H., Gu, Y., Zhang, Y., Yu, X., and Steinmetz, N. F. (2019) Physalis Mottle Virus-like Nanoparticles for Targeted Cancer Imaging. *ACS Appl Mater Interfaces 11*, 18213–18223.
(23) Krishna, S. S., Sastri, M., Savithri, H. S., and Murthy, M. R. (2001) Structural studies on the empty capsids of Physalis mottle virus. *J. Mol. Biol. 307*, 1035–1047.
(24) Umashankar, M., Murthy, M. R. N., Singh, S. A., Appu Rao, A. G., and Savithri, H. S. (2006) The role of inter-subunit ionic interactions in the assembly of Physalis mottle tymovirus. *Arch. Virol. 151*, 1917–1931.
(25) Chandran, D., Shahana, P. V., Rani, G. S., Sugumar, P., Shankar, C. R., and Srinivasan, V. A. (2009) Display of neutralizing epitopes of Canine parvovirus and a T-cell epitope of the fusion protein of Canine distemper virus on chimeric tymovirus-like particles and its use as a vaccine candidate both against Canine parvo and Canine distemper. *Vaccine 28*, 132–139.
(26) Shahana, P. V., Das, D., Gontu, A., Chandran, D., and Maithal, K. (2015) Efficient production of Tymovirus like particles displaying immunodominant epitopes of Japanese Encephalitis Virus envelope protein. *Protein Expr Purif 113*, 35–43.
(27) Masarapu, H., Patel, B. K., Chariou, P. L., Hu, H., Gulati, N. M., Carpenter, B. L., Ghiladi, R. A., Shukla, S., and Steinmetz, N. F. (2017) Physalis Mottle Virus-Like Particles as Nanocarriers for Imaging Reagents and Drugs. *Biomacromolecules 18*, 4141–4153.
(28) Krishna, S. S., Hiremath, C. N., Munshi, S. K., Prahadeeswaran, D., Sastri, M., Savithri, H. S., and Murthy, M. R. (1999) Three-dimensional structure of physalis mottle virus: implications for the viral assembly. *J. Mol. Biol. 289*, 919–934.
(29) Hu, H., and Steinmetz, N. F. (2020) Cisplatin Prodrug-Loaded Nanoparticles Based on Physalis Mottle Virus for Cancer Therapy. *Mol Pharm 17*, 4629–4636.
(30) Hu, H., and Steinmetz, N. F. (2020) Doxorubicin-Loaded Physalis Mottle Virus Particles Function as a pH-Responsive Prodrug Enabling Cancer Therapy. *Biotechnol J 15*, e2000077.
(31) Gao, X., Dong, X., Li, X., Liu, Z., and Liu, H. (2020) Prediction of disulfide bond engineering sites using a machine learning method. *Sci Rep 10*, 10330–9.
(32) Britto, P. J., Knipling, L., and Wolff, J. (2002) The local electrostatic environment determines cysteine reactivity of tubulin. *Journal of Biological Chemistry 277*, 29018–29027.
(33) Barkovich, K. J., Zhao, Z., and Steinmetz, N. F. (2023) iRGD-Targeted Physalis Mottle Virus Like Nanoparticles for Targeted Cancer Delivery. *Small Science* 1–10.
(34) Bai, R., Pettit, G. R., and Hamel, E. (1990) Dolastatin 10, a powerful cytostatic peptide derived from a marine animal. Inhibition of tubulin polymerization mediated through the vinca alkaloid binding domain. *Biochem Pharmacol 39*, 1941–1949.

(35) Shukla, S., Roe, A. J., Liu, R., Veliz, F. A., Commandeur, U., Wald, D. N., and Steinmetz, N. F. (2020) Affinity of plant viral nanoparticle potato virus X (PVX) towards malignant B cells enables cancer drug delivery. *Biomater Sci 8*, 3935–3943.
(36) Kernan, D. L., Wen, A. M., Pitek, A. S., and Steinmetz, N. F. (2017) Delivery of chemotherapeutic vcMMAE using tobacco mosaic virus nanoparticles. *Exp Biol Med (Maywood) 242*, 1405–1411.
(37) Caravan, P., Ellison, J. J., McMurry, T. J., and Lauffer, R. B. (1999) Gadolinium(III) Chelates as MRI Contrast Agents: Structure, Dynamics, and Applications. *Chem. Rev. 99*, 2293–2352.
(38) Wahsner, J., Gale, E. M., Rodríguez-Rodríguez, A., and Caravan, P. (2019) Chemistry of MRI Contrast Agents: Current Challenges and New Frontiers. *Chem. Rev. 119*, 957–1057.
(39) Hagberg, G. E., and Scheffler, K. (2013) Effect of r_1 and r_2 relaxivity of gadolinium-based contrast agents on the T_1-weighted MR signal at increasing magnetic field strengths. *Contrast Media Mol Imaging 8*, 456–465.
(40) Bin Na, H., Song, I. C., and Hyeon, T. (2009) Inorganic Nanoparticles for MRI Contrast Agents. *Advanced Materials 21*, 2133–2148.
(41) Caravan, P. (2006) Strategies for increasing the sensitivity of gadolinium based MRI contrast agents. *Chem Soc Rev 35*, 512–523.
(42) Gibson, D. G., Young, L., Chuang, R.-Y., Venter, J. C., Hutchison, C. A., and Smith, H. O. (2009) Enzymatic assembly of DNA molecules up to several hundred kilobases. *Nat. Methods 6*, 343–345.
(43) Pettersen, E. F., Goddard, T. D., Huang, C. C., Couch, G. S., Greenblatt, D. M., Meng, E. C., and Ferrin, T. E. (2004) UCSF Chimera--a visualization system for exploratory research and analysis. *J Comput Chem 25*, 1605–1612.
(44) Shapovalov, M. V., and Dunbrack, R. L. (2011) A smoothed backbone-dependent rotamer library for proteins derived from adaptive kernel density estimates and regressions. *Structure 19*, 844–858.
(45) Schindelin, J., Arganda-Carreras, I., Frise, E., Kaynig, V., Longair, M., Pietzsch, T., Preibisch, S., Rueden, C., Saalfeld, S., Schmid, B., Tinevez, J.-Y., White, D. J., Hartenstein, V., Eliceiri, K., Tomancak, P., and Cardona, A. (2012) Fiji: an open-source platform for biological-image analysis. *Nat. Methods 9*, 676–682.